EUROPEAN ORGANIZATION FOR NUCLEAR RESEARCH

L3 Note 2756
June 26, 2002

Preliminary Results on the Measurement of W-Pair Cross Sections in e^+e^- Interactions at $\sqrt{s} = 205 - 208$ GeV and W-Decay Branching Fractions

The L3 Collaboration

Abstract

We report on the measurement of W-boson pair-production with the L3 detector at LEP. In a data sample corresponding to a total luminosity of 217.3 pb^{-1} collected at centre-of-mass energies ranging from 205 to 208 GeV, we select 3528 four-fermion events with pairs of hadronic jets or pairs of leptons with high invariant masses. Branching fractions of W decays into different fermion-antifermion pairs are determined including data collected at lower centre-of-mass energies. Assuming charged-current lepton universality, the branching fraction for hadronic W decays is measured to be: $B(\mathrm{W} \rightarrow \mathrm{hadrons}) = 68.34 \pm 0.40\ (stat.) \pm 0.33\ (syst.)\ \%$. Differential cross sections as a function of the W^- scattering angle are also derived using the full collected statistics in the semileptonic channels $qqe\nu(\gamma)$ and $qq\mu\nu(\gamma)$. These results are preliminary.

Submitted to the 31^{st} *International Conference on High Energy Physics*
Amsterdam, Netherlands, 24-31 July 2002.

1 Introduction

For the year 2000 data taking period, the centre-of-mass energy, $\sqrt{s}$, of the $\mathrm{e^+e^-}$ collider LEP at CERN was increased in several steps from 200 GeV to 208 GeV. These energies are well above the kinematic threshold of W-boson pair production, $\mathrm{e^+e^-} \to \mathrm{W^+W^-}$.

To lowest order within the Standard Model [1], three Feynman diagrams contribute to W-pair production, the s-channel γ and Z-boson exchange and the t-channel ν_{e} exchange, referred to as CC03 [2–4]. The W boson decays into a quark-antiquark pair, for example $\mathrm{W^-} \to \bar{\mathrm{u}}\mathrm{d}$ or $\bar{\mathrm{c}}\mathrm{s}$, or a lepton-antilepton pair, $\mathrm{W^-} \to \ell^-\bar{\nu}_\ell$ ($\ell = \mathrm{e}, \mu, \tau$); in the following denoted as qq, $\ell\nu$ or ff in general for both $\mathrm{W^+}$ and $\mathrm{W^-}$ decays. In this letter, measurements of all four-fermion final states mediated by W-pair production are reported:

1. $\mathrm{e^+e^-} \to \ell\nu\ell\nu(\gamma)$
2. $\mathrm{e^+e^-} \to qq\mathrm{e}\nu(\gamma)$
3. $\mathrm{e^+e^-} \to qq\mu\nu(\gamma)$
4. $\mathrm{e^+e^-} \to qq\tau\nu(\gamma)$
5. $\mathrm{e^+e^-} \to qqqq(\gamma)$,

where (γ) indicates the possible presence of radiative photons. Additional contributions to the production of four-fermion final states arising from other neutral-current (NC) or charged-current (CC) Feynman diagrams are small. At the current level of statistical accuracy the interference effects need to be taken into account only for $\mathrm{e^+e^-} \to \ell\nu\ell\nu(\gamma)$ (CC56+NC56) and $\mathrm{e^+e^-} \to qq\mathrm{e}\nu(\gamma)$ (CC20) [2–4].

For cross section measurements, the collected luminosity has been split in three centre-of-mass bins: 78.9 $\mathrm{pb^{-1}}$ at $\sqrt{s} < 205.8$ GeV (hereafter called 205 and having in average $\langle\sqrt{s}\rangle = 204.82$ GeV); 129.8 $\mathrm{pb^{-1}}$ at $205.8 < \sqrt{s} < 207.2$ GeV (hereafter called 206 and having in average $\langle\sqrt{s}\rangle = 206.48$ GeV) and 8.5 $\mathrm{pb^{-1}}$ at $\sqrt{s} > 207.2$ GeV (hereafter called 208 and having in average $\langle\sqrt{s}\rangle = 208.00$ GeV). These centre-of-mass energies are known to ± 0.05 GeV [5].

The cross section is measured for all four-fermion final states mediated by W-pair production. Combining these preliminary measurements, W-decay branching fractions and the total W-pair production cross section are determined with improved precision compared to earlier measurements with less luminosity reported by L3 [6–10] and other LEP experiments [11]. The differential cross section as a function of the $\mathrm{W^-}$ scattering angle is also derived using the full statistics collected by the L3 experiment in the $qq\mathrm{e}\nu(\gamma)$ and $qq\mu\nu(\gamma)$ final states.

2 Analysis of Four-Fermion Production

The L3 detector is described in detail in Reference 12. The selections of the four-fermion final states are similar to the ones used at lower centre-of-mass energies [6–10]. Charged leptons are explicitly identified using their characteristic signature. In general, electrons are identified as energy depositions in the BGO electromagnetic calorimeter with electromagnetic shower shape which are matched in azimuth to a track reconstructed in the central tracking chamber (TEC). Muons are identified either as tracks reconstructed in the muon chambers pointing back to the interaction vertex or by their minimum-ionising-particle (MIP) signature. Jets arising from hadronic τ decays are reconstructed based on a jet-clustering inside a cone of 15° half-opening angle [13]. Hadronic jets corresponding to quarks are reconstructed using the Durham jet algorithm [14]. The momentum of the neutrino in $\mathrm{e^+e^-} \to qq\ell\nu$ events is identified with the missing momentum vector.

Selection efficiencies and background contaminations of all processes are determined by

Monte Carlo simulations. The following Monte Carlo event generators are used to simulate the various signal and background processes: KORALW [15] and HERWIG [16] ($e^+e^- \rightarrow WW \rightarrow ffff(\gamma)$); EXCALIBUR [17] ($e^+e^- \rightarrow ffff(\gamma)$); PYTHIA [18] ($e^+e^- \rightarrow q\bar{q}(\gamma), ZZ(\gamma)$); KORALZ [19] ($e^+e^- \rightarrow \mu^+\mu^-(\gamma)$, $\tau^+\tau^-(\gamma)$); BHAGENE3 [20], BHWIDE [21] and TEEGG [22] ($e^+e^- \rightarrow e^+e^-(\gamma)$), DIAG36 [23] and LEP4F [24] (leptonic two-photon collisions); PHOJET [25] (hadronic two-photon collisions). The response of the L3 detector is modelled with the GEANT [26] detector simulation program which includes the effects of energy loss, multiple scattering and showering in the detector material. Hadronic showers are simulated with the GHEISHA [27] program.

The measurement of the total luminosity, $\mathcal{L}$, follows the procedure described in Reference 28. The preliminary total error on the luminosity measurement for the 2000 data is estimated to be 0.61%.

The results on cross sections and W-decay branching fractions are determined in a combined analysis taking migration between the various final states into account [6–10]. The results are compared to the predictions of the Standard Model calculated for a mass of the W boson of $M_W = 80.35$ GeV using the YFSWW3 [29] and RacoonWW [30] programs.

2.1 $e^+e^- \rightarrow \ell\nu\ell\nu(\gamma)$

The event selection for the process $e^+e^- \rightarrow \ell\nu\ell\nu(\gamma)$ requires two charged leptons and missing energy due to the neutrinos. The selection depends on whether the event contains zero, one or two identified electrons or muons, referred to as jet-jet, lepton-jet and lepton-lepton class. Electrons, muons and τ jets are identified inside the polar angular range of $|\cos\theta| < 0.96$. For events with one or two electrons, one electron should lie in the angular range $|\cos\theta| < 0.92$ in order to limit the amount of background from Bhabha scattering. For events containing jets only, the two highest energy jets must also satisfy $|\cos\theta| < 0.92$.

A total of 234 events is selected in the data: 150 lepton-lepton events, 68 lepton-jet events and 16 jet-jet events. The distributions of the acoplanarity between the two charged leptons for lepton-lepton events, and of the transverse energy imbalance normalized to the visible energy are shown in Figure 1.

The signal efficiencies are determined from CC56+NC56 Monte Carlo samples within the following phase-space cuts: $|\cos\theta| < 0.96$ for both charged leptons, with energies larger than 15 GeV and 5 GeV, respectively. Efficiencies are given in the form of a 6 by 6 matrix, as shown in Table 1, relating $\ell\nu\ell\nu$ events at four-fermion level to $\ell\nu\ell\nu$ events at reconstruction level. The background contributions are listed in Table 2. A total systematic error of 4.7% on the measured cross section is obtained.

2.2 $e^+e^- \rightarrow qqe\nu(\gamma)$

The event selection for the process $e^+e^- \rightarrow qqe\nu(\gamma)$ requires an identified electron of at least 20 GeV, high particle multiplicity arising from the $q\bar{q}$ system, and missing momentum due to the neutrino.

A total of 491 events is selected in the data: 473 events with the electron identified in the BGO electromagnetic calorimeter and 18 events with the electron identified in the SPACAL calorimeter. The distributions of the energy of the electron and the invariant mass of the electron-neutrino system are shown in Figure 2.

The signal efficiency is determined from a CC20 Monte Carlo sample within the following phase-space cuts: $E_{\mathrm{e}}, E_\nu > 15$ GeV; $|\cos\theta_{\mathrm{e}}|, |\cos\theta_\nu| < 0.98$; $M_{\mathrm{e}\nu}, M_{qq} > 45$ GeV. The selection efficiencies and the background contributions are listed in Tables 1 and 2. A total systematic error of 2.0% on the measured cross section is obtained.

2.3 $\mathrm{e^+e^-} \rightarrow qq\mu\nu(\gamma)$

The event selection for the process $\mathrm{e^+e^-} \rightarrow qq\mu\nu(\gamma)$ requires high particle multiplicity arising from the $q\bar{q}$ system, an identified muon and missing momentum due to the neutrino.

A total of 427 events is selected in the data: 381 events with a muon reconstructed in the muon spectrometer and 46 events with a muon identified by its MIP signature. The distributions of the momentum of the muon and the invariant mass of the jet-jet system are shown in Figure 3. The selection efficiencies and background contribution are listed in Tables 1 and 2. A total systematic error of 3.0% on the measured cross section is obtained.

2.4 $\mathrm{e^+e^-} \rightarrow qq\tau\nu(\gamma)$

The event selection for the process $\mathrm{e^+e^-} \rightarrow qq\tau\nu(\gamma)$ is based on the identification of a tau jet in a hadronic event with missing energy.

A total of 480 events is selected in the data: 60 $\tau \rightarrow \nu \mathrm{e} \bar{\nu}$ events, 63 $\tau \rightarrow \nu\mu\bar{\nu}$ events and 357 $\tau \rightarrow \nu$hadrons events. The distributions of the number of TEC tracks associated to the τ jet and of the invariant mass of the $\tau\nu$ system are shown in Figure 4. The selection efficiencies and the background contributions are listed in Tables 1 and 2. A total systematic error of 4.3% on the measured cross section is obtained.

2.5 $\mathrm{e^+e^-} \rightarrow qqqq(\gamma)$

The event selection for the process $\mathrm{e^+e^-} \rightarrow qqqq(\gamma)$ is based on a neural network applied to a sample of pre-selected events. The pre-selection accepts 92% of the $\mathrm{WW} \rightarrow qqqq(\gamma)$ signal. The network is trained such that the output peaks at one for the signal and at zero for the background. The distribution of the neural-network output is shown in Figure 6.

The neural-network output distribution for data events is fitted by a linear combination of neural-network output distributions derived from Monte Carlo simulations for signal and background [6–10]. The results of the fit for the signal cross sections are shown in Table 3, as well as in Table 5. The results for the $\mathrm{e^+e^-} \rightarrow q\bar{q}(\gamma)$ background cross sections at the three centre-of-mass energies are 87.2 ± 5.3 pb, 80.3 ± 4.0 pb and 77.9 ± 15.8 pb respectively, where the errors are only statistical. These values are in good agreement with the Standard Model prediction.

As a cross check the signal cross section is determined by applying a cut on the output of the neural network larger than 0.8, which minimises the expected statistical error. The selection efficiencies (at $\sqrt{s} = 207$ GeV) and the background contributions corresponding to this cut are listed in Tables 1 and 2. A total of 1896 events is selected in the data, yielding signal cross sections at the three centre-of-mass energies of 8.15 ± 0.39 pb, 8.53 ± 0.31 pb and 8.32 ± 1.19 pb respectively, in good agreement with the results of the fit to the neural-network output distribution. A total systematic error of 1.8% on the measured cross section is obtained.

3 Results

The cross sections, σ_i, of the signal processes i are determined simultaneously in one maximum-likelihood fit, taking cross feed between final states into account. The fitting procedure to determine cross sections of the signal processes, W-decay branching fractions and the total W-pair cross section is identical to the one used previously [6–10].

For the purely leptonic final states the fitting procedure determines six different cross sections corresponding to all possible combinations of flavours of the two final-state lepton pairs. Since the data statistics for the $\ell\nu\ell\nu(\gamma)$ final state is low, the sum of these six cross sections is quoted as the cross section for the process $\mathrm{e^+e^-} \rightarrow \ell\nu\ell\nu(\gamma)$.

The total likelihood is given by the product of Poissonian probabilities, $P(N_i, \mu_i)$, corresponding to the signal processes i having N_i selected events as listed in Table 2. The expected number of events for process i, μ_i, is calculated as:

$$\mu_i \quad = \quad \left(\sum_{j=1}^{10} \epsilon_{ij} \sigma_j + \sigma_i^{\mathrm{bg}} \right) \cdot \mathcal{L} \, , \tag{1}$$

where ϵ_{ij} is the efficiency of selection i to accept events from process j, σ_i^{bg} is the remaining background cross section arising from other processes. These numbers are listed in Tables 1 and 2. For the $\mathrm{e^+e^-} \rightarrow qqqq(\gamma)$ process, the Poissonian probability is replaced by the likelihood as a function of the signal cross section derived from the fit described in Section 2.5.

3.1 Signal Cross Sections

For the $qq\mathrm{e}\nu(\gamma)$ and the six $\ell\nu\ell\nu(\gamma)$ final states the cross sections are determined within phase-space cuts to reduce contributions from processes not mediated by resonant W-pair production. In order to determine W-pair cross sections for these final states the measured cross sections are scaled by a multiplicative factor, f_i, as listed in Table 2. The conversion factors f_i are given by the ratio of the total CC03 cross section and the four-fermion cross section within phase-space cuts, and are calculated within the Standard Model using EXCALIBUR.

The resulting cross sections including statistical and systematic errors are listed in Table 3. The Standard Model agrees well with these results. Since the efficiency matrix of Table 1 contains non-zero off-diagonal elements, the five cross sections are correlated. The largest correlations, -13% and -17%, arise among the semileptonic channels between $qq\tau\nu$ and $qq\mathrm{e}\nu$ and between $qq\tau\nu$ and $qq\mu\nu$. All other correlations are smaller than 1% in magnitude and thus negligible.

3.2 W-Decay Branching Fractions and W-Pair Cross Section

For the determination of the total CC03 production cross section of W-pairs, σ_{WW}, the signal cross sections σ_i are replaced by the product $r_i\sigma_{\mathrm{WW}}$ or $r_i\sigma_{\mathrm{WW}}/f_i$ for the $qq\mathrm{e}\nu(\gamma)$ and $\ell\nu\ell\nu(\gamma)$ final states. The ratios r_i are given in terms of the W-decay branching fractions, $B(\mathrm{W} \rightarrow qq)$ and $B(\mathrm{W} \rightarrow \ell\nu)$, as follows: $r_{qqqq} = [B(\mathrm{W} \rightarrow qq)]^2$, $r_{qq\ell\nu} = 2B(\mathrm{W} \rightarrow qq)B(\mathrm{W} \rightarrow \ell\nu)$, and $r_{\ell\nu\ell\nu} = [B(\mathrm{W} \rightarrow \ell\nu)]^2$ for identical and $r_{\ell\nu\ell'\nu'} = 2B(\mathrm{W} \rightarrow \ell\nu)B(\mathrm{W} \rightarrow \ell'\nu')$ for different lepton flavours in the final state. The sum of the hadronic and the three leptonic branching fractions is constrained to be unity. For the determination of W-decay branching fractions the data collected at lower centre-of-mass energies are included.

The resulting W-decay branching fractions including statistical and systematic errors and correlations are listed in Table 4. The branching fractions are determined both with and without the assumption of charged-current lepton universality in W decays. Assuming lepton universality, the hadronic W-decay branching fraction is:

$$B(\mathrm{W} \to qq) \quad = \quad 68.34 \pm 0.40 \pm 0.33\ \%\,, \tag{2}$$

where the first error is statistical and the second systematic. The accuracy on the W-decay branching fractions is significantly improved with respect to our previous publications [6–10].

The branching fractions of the W boson depend on the six elements V_{ij} of the Cabibbo-Kobayashi-Maskawa quark mixing matrix V_{CKM} [31] not involving the top quark [3], $1/B(\mathrm{W} \to \ell\nu) = 3 + 3[1 + \alpha_{\mathrm{s}}(M_{\mathrm{W}})/\pi]V^2$, where α_{s} is the strong coupling constant. Our measurements correspond to:

$$V^2 \quad = \sum_{i=\mathrm{u,c};\, j=\mathrm{d,s,b}} |V_{ij}|^2 \quad = \quad 2.079 \pm 0.038 \pm 0.032\,. \tag{3}$$

The sensitivity of this measurement to a single matrix element is largest for the dominant diagonal elements of V_{CKM}. Since V_{ud} is known much more precisely than V_{cs}, it is most useful to determine the latter. Using the current world-average values and errors of the other matrix elements not assuming the unitarity of V_{CKM} [32], the result is:

$$|V_{\mathrm{cs}}| \quad = \quad 1.014 \pm 0.019 \pm 0.015\,. \tag{4}$$

The statistical error includes the errors on α_{s} and the other V_{ij} but is dominated by the statistical error on the W branching fractions.

The W-pair cross sections are also derived imposing the W-decay branching fractions as expected within the Standard Model [3]. Results for the cross sections of the reactions $\mathrm{e^+e^-} \to \ell\nu\ell\nu(\gamma)$, $\mathrm{e^+e^-} \to qq\ell\nu(\gamma)$, $\mathrm{e^+e^-} \to qqqq(\gamma)$, and the total W-pair cross section, σ_{WW}, are shown in Table 5. The results for the total production cross section of W-pairs at the three centre-of-mass energies are:

$$\sqrt{s} = 204.82 \pm 0.05\ \mathrm{GeV}: \qquad \sigma_{\mathrm{WW}} = 17.35 \pm 0.58 \pm 0.24\ \mathrm{pb}\,, \tag{5}$$
$$\sqrt{s} = 206.48 \pm 0.05\ \mathrm{GeV}: \qquad \sigma_{\mathrm{WW}} = 17.91 \pm 0.46 \pm 0.24\ \mathrm{pb}\,, \tag{6}$$
$$\sqrt{s} = 208.00 \pm 0.05\ \mathrm{GeV}: \qquad \sigma_{\mathrm{WW}} = 18.69 \pm 1.83 \pm 0.24\ \mathrm{pb}\,. \tag{7}$$

Our published measurements of σ_{WW} at $\sqrt{s}$ of 161 GeV, 172 GeV, 183 GeV, 189 GeV, our preliminary results at $\sqrt{s} = 192-202$ GeV, and the new preliminary results at $\sqrt{s} = 205-208$ GeV presented here are compared to the Standard Model expectation in Figure 7 as calculated with the Monte Carlo programs YFSWW3 [29] in the whole energy range and RacoonWW [30] for $\sqrt{s} \geq 170$ GeV. The two predictions are consistent and have a theoretical uncertainty of 2.0% in the threshold region going down to 0.5% [3,4] for $\sqrt{s} \geq 170$ GeV where the DPA approximation is used.

3.3 Differential Cross Section

Using the data sample described in Section 2, we have derived the differential cross-section measurement as a function of the $\cos\theta_{\mathrm{W^-}}$ combining the semileptonic channels $qqe\nu(\gamma)$ and $qq\mu\nu(\gamma)$ in a restricted phase space region.

The $qq\tau\nu(\gamma)$ and $qqqq(\gamma)$ final states are not used because of the less performant charge assignment, of the ambiguity on the association of the jets to single W-bosons and of the larger background contamination. The $\ell\nu\ell\nu(\gamma)$ final state cannot be used due to the W direction ambiguity caused by the presence of two or more neutrinos.

The $\mathrm{d}\sigma/\mathrm{d}(\cos\theta_{\mathrm{W}^-})$ measurements are combined in ten bins of $\cos\theta_{\mathrm{W}^-}$ for both the $qq\mu\nu(\gamma)$ and $qqe\nu(\gamma)$ channels inside the following energy bins:

$$180.0 - 184.0 \text{ GeV}, \;\; 184.0 - 194.0 \text{ GeV}$$
$$194.0 - 204.0 \text{ GeV}, \;\; 204.0 - 210.0 \text{ GeV} \; .$$

The energy ranges are chosen such that bias effects due to the non-linear evolution of the $\mathrm{d}\sigma/\mathrm{d}(\cos\theta_{\mathrm{W}^-})$ with $\sqrt{s}$ are minimized. The generated $\cos\theta_{\mathrm{W}^-}$ angle is defined following the ECAL05 $\gamma-$recombination scheme [33]. Moreover, the measured cross-section is corrected to the CC03 set of diagrams with the additional restriction of $\theta_{\ell^\pm} > 20^\circ$ where $\theta_{\ell^\pm}$ is the angle between the charged lepton and the beam direction. The observed distributions are corrected using a simplified bin-by-bin and background factor.

The cross section for each $\cos\theta_{\mathrm{W}^-}$ bin is calculated using the formula:

$$\sigma_i = \frac{N_i - b_i}{f_i \mathcal{L}}, \quad i = 1, 10$$

where $\mathcal{L}$ is the integrated luminosity, N_i is the number of selected events in the i-*th* bin, b_i is the amount of expected background contamination in the same bin and f_i is the correction factor which takes into account the selection efficiency and the bin-to-bin migration effects. Both b_i and f_i are derived from Monte Carlo simulations.

The usage of a bin-by-bin correction makes the resulting σ_i largely uncorrelated, nonetheless the residual correlations might induce biases in case of deviation from Standard Model. In order to evaluate the possible biases, a non-Standard Model $\cos\theta_{\mathrm{W}^-}$ distribution has been generated using the following re-weighting function:

$$f(\theta) = 0.2 \cdot \cos\theta_{\mathrm{W}^-} + 1$$

starting from a Standard Model Monte Carlo. These modified distributions are used as a fake data sample. The comparison between the re-weighted sample and the signal Standard Model distribution is shown in Figure 8 at $\sqrt{s} = 189$ GeV for the $qq\mu\nu(\gamma)$ channel. The agreement between the fake data sample after reconstruction and the modified Monte Carlo distribution is good, showing no appreciable bias in the method.

Another bias could arise directly from the WW Monte Carlo Generator used to estimate the efficiency correction. This possible additional systematics is tested comparing the $\cos\theta_{\mathrm{W}^-}$ distributions obtained using both KORALW [15] and YFSWW3 [29] Monte Carlo Generators. The discrepancy between the predictions from the two generators is negligible.

Charge confusion effects, which might affect the reconstruction of W-boson direction, are taken into account. The residual uncertainty obtained comparing data and Monte Carlo expectations on the Z-peak sample, is considered as a systematics.

Other sources of systematics uncertainties are considered in analogy with the total WW cross section analysis.

The differential distributions, averaging the $qqe\nu(\gamma)$ and $qq\mu\nu(\gamma)$ channels, are shown in Figure 9 for the four defined energy ranges. The errors include both statistical and systematics components

4 Acknowledgments

We wish to congratulate the CERN accelerator divisions for the successful upgrade of the LEP machine and to express our gratitude for its excellent performance. We acknowledge with appreciation the effort of the engineers, technicians and support staff who have participated in the construction and maintenance of this experiment.

References

[1] S. L. Glashow, Nucl. Phys. **22** (1961) 579;
S. Weinberg, Phys. Rev. Lett. **19** (1967) 1264;
A. Salam, in *Elementary Particle Theory*, ed. N. Svartholm, Stockholm, Almquist and Wiksell (1968), 367.

[2] D. Bardin *et al.*, Nucl. Phys. (Proc. Suppl.) **B 37** (1994) 148;
F.A. Berends *et al.*, Nucl. Phys. (Proc. Suppl.) **B 37** (1994) 163.

[3] W. Beenakker *et al.*, in *Physics at LEP 2*, Report CERN 96-01 (1996), eds G. Altarelli, T. Sjöstrand, F. Zwirner, Vol. 1, p. 79.

[4] D. Bardin *et al.*, in *Physics at LEP 2*, Report CERN 96-01 (1996), eds G. Altarelli, T. Sjöstrand, F. Zwirner, Vol. 2, p. 3.

[5] The LEP Energy Working Group, Private communication.

[6] The L3 Collaboration, M. Acciarri *et al.*, Phys. Lett. **B 398** (1997) 223.

[7] The L3 Collaboration, M. Acciarri *et al.*, Phys. Lett. **B 407** (1997) 419.

[8] The L3 Collaboration, M. Acciarri *et al.*, Phys. Lett. **B 436** (1998) 437.

[9] The L3 Collaboration, M. Acciarri *et al.*, Phys. Lett. **B 496** (2000) 19.

[10] The W-Physics Analysis Group of the L3 Collaboration,
Preliminary Results on the Measurement of W-Pair Cross Sections in e^+e^- *Interactions at* $\sqrt{(s)} = 192-202$ *GeV and W-Decay Branching Fractions*, L3 Note 2514, June 2000; paper #512-(PL/PA 6a/5) submitted to the XXXth International Conference on High Energy Physics – 27 July-2 August 2000, Osaka, Japan.

[11] The ALEPH Collaboration, R. Barate *et al.*, Phys. Lett. **B 401** (1997) 347, Phys. Lett. **B 415** (1997) 435, Phys. Lett. **B 453** (1999) 107, Phys. Lett. **B 484** (2000) 205;
The DELPHI Collaboration, P. Abreu *et al.*, Phys. Lett. **B 397** (1997) 158, Euro. Phys. Jour. **C 2** (1998) 581, Phys. Lett. **B 456** (1999) 310, Phys. Lett. **B 479** (2000) 89;
The OPAL Collaboration, K. Ackerstaff *et al.*, Phys. Lett. **B 389** (1996) 416, Euro. Phys. Jour. **C 1** (1998) 425, Euro. Phys. Jour. **C 8** (1999) 191, Phys. Lett. **B 493** (2000) 249.

[12] The L3 Collaboration, B. Adeva *et al.*, Nucl. Instr. and Meth. **A 289** (1990) 35;
M. Chemarin *et al.*, Nucl. Instr. and Meth. **A 349** (1994) 345;
M. Acciarri *et al.*, Nucl. Instr. and Meth. **A 351** (1994) 300;
G. Basti *et al.*, Nucl. Instr. and Meth. **A 374** (1996) 293;
I.C. Brock *et al.*, Nucl. Instr. and Meth. **A 381** (1996) 236;
A. Adam *et al.*, Nucl. Instr. and Meth. **A 383** (1996) 342.

[13] H.J. Daum *et al.*, Z. Phys. **C 8** (1981) 167.

[14] S. Catani *et al.*, Phys. Lett. **B 269** (1991) 432;
S. Bethke *et al.*, Nucl. Phys. **B 370** (1992) 310.

[15] KORALW version 1.42 is used.
M. Skrzypek, S. Jadach, W. Placzek and Z. Wąs, Comp. Phys. Comm. **94** (1996) 216;
M. Skrzypek, S. Jadach, M. Martinez, W. Placzek and Z. Wąs, Phys. Lett. **B 372** (1996) 289;
S. Jadach, W. Placzek, M. Skrzypek, B.F.L. Ward and Z. Wąs, CERN-TH/98-242.

[16] HERWIG version 5.9 is used.
G. Marchesini and B. Webber, Nucl. Phys. **B 310** (1988) 461;
I.G. Knowles, Nucl. Phys. **B 310** (1988) 571;
G. Marchesini *et al.*, Comp. Phys. Comm. **67** (1992) 465.

[17] F.A. Berends, R. Kleiss and R. Pittau, Nucl. Phys. **B 424** (1994) 308; Nucl. Phys. **B 426** (1994) 344; Nucl. Phys. (Proc. Suppl.) **B 37** (1994) 163;
R. Kleiss and R. Pittau, Comp. Phys. Comm. **83** (1994) 141;
R. Pittau, Phys. Lett. **B 335** (1994) 490.

[18] PYTHIA version 5.722 is used.
T. Sjöstrand, *PYTHIA 5.7 and JETSET 7.4 Physics and Manual*,
CERN-TH/7112/93 (1993), revised August 1995; Comp. Phys. Comm. **82** (1994) 74.

[19] KORALZ version 4.02 is used.
S. Jadach, B. F. L. Ward and Z. Wąs, Comp. Phys. Comm. **79** (1994) 503.

[20] J.H. Field, Phys. Lett. **B 323** (1994) 432;
J.H. Field and T. Riemann, Comp. Phys. Comm. **94** (1996) 53.

[21] BHWIDE version 1.01 is used.
S. Jadach, W. Placzek, B.F.L. Ward, Phys. Rev. **D 40** (1989) 3582, Comp. Phys. Comm. **70** (1992) 305, Phys. Lett. **B 390** (1997) 298.

[22] D. Karlen, Nucl. Phys. **B 289** (1987) 23.

[23] F. A. Berends, P. H. Daverfeldt and R. Kleiss, Nucl. Phys. **B 253** (1985) 441.

[24] J.A.M. Vermaseren, J. Smith and G. Grammer Jr, Phys. Rev. **D 19** (1979) 137;
J.A.M. Vermaseren, Nucl. Phys. **B 229** (1983) 347.

[25] PHOJET version 1.05 is used.
R. Engel, Z. Phys. **C 66** (1995) 203; R. Engel and J. Ranft, Phys. Rev. **D 54** (1996) 4244.

[26] The L3 detector simulation is based on GEANT Version 3.15.
R. Brun *et al.*, *GEANT 3*, CERN-DD/EE/84-1 (Revised), 1987.
The GHEISHA program (H. Fesefeldt, RWTH Aachen Report PITHA 85/02 (1985)) is used to simulate hadronic interactions.

[27] H. Fesefeldt, RWTH Aachen Preprint PITHA 85/02 (1985).

[28] The L3 Collaboration, I.C. Brock *et al.*, Nucl. Instr. and Meth. **A 381** (1996) 236.

[29] S. Jadach *et al.*, Phys. Lett. **B 417** (1998) 326;
Phys. Rev. **D61** (2000) 113010;
UTHEP-00-0101, CERN-TH/2000-337, *hep-ph/0007012* to be subm. to Phys. Lett. **B**.

[30] A. Denner *et al.*, Nucl. Phys. **B 587** (2000) 67, *hep-ph/0006307*.

[31] N. Cabibbo, Phys. Rev. Lett. **10** (1963) 531;
M. Kobayashi and T. Maskawa, Prog. Theor. Phys. **49** (1973) 652.

[32] D.E. Groom *et al.*, *The 2000 Review of Particle Physics*, Euro. Phys. Jour. **C 15** (2000) 1.

[33] M. W. Grünewald *et al.*, in LEP2 Monte Carlo Workshop: Report of the Working Groups on Precision Calculations for LEP2 Physics, *hep-ph/0005309*.

Selection of Process	Efficiencies [%] for									
	$e\nu e\nu$	$e\nu\mu\nu$	$e\nu\tau\nu$	$\mu\nu\mu\nu$	$\mu\nu\tau\nu$	$\tau\nu\tau\nu$	$qqe\nu$	$qq\mu\nu$	$qq\tau\nu$	$qqqq$
$e^+e^- \to e\nu e\nu(\gamma)$	63.1	0.3	12.6			1.6				
$e^+e^- \to e\nu\mu\nu(\gamma)$		57.7	10.0	0.6	10.9	1.9				
$e^+e^- \to e\nu\tau\nu(\gamma)$	5.3	1.1	33.5		0.2	6.9				
$e^+e^- \to \mu\nu\mu\nu(\gamma)$				50.1	8.6	0.6				
$e^+e^- \to \mu\nu\tau\nu(\gamma)$		2.4	0.3	1.9	28.4	4.8				
$e^+e^- \to \tau\nu\tau\nu(\gamma)$	0.2	0.1	1.9		0.9	18.8				
$e^+e^- \to qqe\nu(\gamma)$							81.9	0.2	2.3	
$e^+e^- \to qq\mu\nu(\gamma)$							0.2	73.5	3.6	
$e^+e^- \to qq\tau\nu(\gamma)$							6.3	7.7	50.1	0.1
$e^+e^- \to qqqq(\gamma)$							0.1		0.5	84.3

Table 1: Selection efficiencies for signal processes $e^+e^- \to \ell\nu\ell\nu(\gamma)$, $e^+e^- \to qq\ell\nu(\gamma)$, and $e^+e^- \to qqqq(\gamma)$, at $\sqrt{s} = 207$ GeV. For the $\ell\nu\ell\nu$ ($qqe\nu$) selections, the signal efficiency is derived from a CC56+NC56 (CC20) Monte Carlo sample and is given within phase-space cuts, see Section 2.1 (2.2). For the $qqqq$ selection, the numbers are quoted for a neural-network output larger than 0.8. Selection efficiencies at other centre-of-mass energies are only marginally different.

Selection of Process	205 GeV N_{data}	205 GeV Bg [pb]	207 GeV N_{data}	207 GeV Bg [pb]	208 GeV N_{data}	208 GeV Bg [pb]	f_i
$\mathrm{e^+e^-} \rightarrow \mathrm{e}\nu\mathrm{e}\nu(\gamma)$	29	0.112	30	0.080	2	0.080	0.87
$\mathrm{e^+e^-} \rightarrow \mathrm{e}\nu\mu\nu(\gamma)$	18	0.037	35	0.029	2	0.029	1.08
$\mathrm{e^+e^-} \rightarrow \mathrm{e}\nu\tau\nu(\gamma)$	13	0.040	25	0.024	3	0.024	1.08
$\mathrm{e^+e^-} \rightarrow \mu\nu\mu\nu(\gamma)$	12	0.087	19	0.084	3	0.084	0.96
$\mathrm{e^+e^-} \rightarrow \mu\nu\tau\nu(\gamma)$	11	0.009	14	0.007	2	0.007	1.12
$\mathrm{e^+e^-} \rightarrow \tau\nu\tau\nu(\gamma)$	5	0.013	10	0.009	1	0.009	0.96
$\mathrm{e^+e^-} \rightarrow qq\mathrm{e}\nu(\gamma)$	185	0.145	291	0.119	15	0.122	1.01
$\mathrm{e^+e^-} \rightarrow qq\mu\nu(\gamma)$	152	0.096	252	0.079	23	0.098	—
$\mathrm{e^+e^-} \rightarrow qq\tau\nu(\gamma)$	166	0.385	294	0.360	20	0.366	—
$\mathrm{e^+e^-} \rightarrow qqqq(\gamma)$	674	1.582	1147	1.590	75	1.630	—

Table 2: Number of selected data events, N_{data}, and accepted background cross sections (Bg) from non-W processes for the selections of the signal processes $\mathrm{e^+e^-} \rightarrow \ell\nu\ell\nu(\gamma)$, $\mathrm{e^+e^-} \rightarrow qq\ell\nu(\gamma)$, and $\mathrm{e^+e^-} \rightarrow qqqq(\gamma)$, at the three different centre-of-mass energies. For the $qqqq$ selection, the numbers are quoted for a neural-network output larger than 0.8. The ratio of the CC03 cross section without cuts and the four-fermion cross section within phase-space cuts, f_i, is calculated with EXCALIBUR at $\sqrt{s} = 207$ GeV and listed in the last column; the dependence of these numbers on $\sqrt{s}$ is very small.

Process	N_{data}	N_{bg}	σ(CC03) [pb]	σ_{YFSWW3} [pb]
$\sqrt{s} = 205$ GeV				
$\mathrm{e^+e^-} \to \ell\nu\ell\nu(\gamma)$	88	23.5	$1.56 \pm 0.23 \pm 0.07$	1.82 ± 0.01
$\mathrm{e^+e^-} \to qq\mathrm{e}\nu(\gamma)$	185	11.4	$2.66 \pm 0.22 \pm 0.05$	2.50 ± 0.01
$\mathrm{e^+e^-} \to qq\mu\nu(\gamma)$	152	7.6	$2.35 \pm 0.21 \pm 0.07$	2.50 ± 0.01
$\mathrm{e^+e^-} \to qq\tau\nu(\gamma)$	166	30.4	$2.66 \pm 0.33 \pm 0.11$	2.50 ± 0.01
$\mathrm{e^+e^-} \to qqqq(\gamma)$	674	124.8	$8.06 \pm 0.39 \pm 0.15$	7.81 ± 0.04
$\sqrt{s} = 207$ GeV				
$\mathrm{e^+e^-} \to \ell\nu\ell\nu(\gamma)$	133	30.2	$1.48 \pm 0.17 \pm 0.07$	1.82 ± 0.01
$\mathrm{e^+e^-} \to qq\mathrm{e}\nu(\gamma)$	291	15.5	$2.52 \pm 0.16 \pm 0.05$	2.50 ± 0.01
$\mathrm{e^+e^-} \to qq\mu\nu(\gamma)$	252	10.3	$2.37 \pm 0.17 \pm 0.07$	2.50 ± 0.01
$\mathrm{e^+e^-} \to qq\tau\nu(\gamma)$	294	46.7	$3.09 \pm 0.27 \pm 0.13$	2.50 ± 0.01
$\mathrm{e^+e^-} \to qqqq(\gamma)$	1147	206.4	$8.51 \pm 0.31 \pm 0.15$	7.82 ± 0.04
$\sqrt{s} = 208$ GeV				
$\mathrm{e^+e^-} \to \ell\nu\ell\nu(\gamma)$	13	2.0	$2.44 \pm 0.81 \pm 0.11$	1.82 ± 0.01
$\mathrm{e^+e^-} \to qq\mathrm{e}\nu(\gamma)$	15	0.9	$1.88 \pm 0.55 \pm 0.04$	2.50 ± 0.01
$\mathrm{e^+e^-} \to qq\mu\nu(\gamma)$	23	0.8	$3.29 \pm 0.75 \pm 0.10$	2.50 ± 0.01
$\mathrm{e^+e^-} \to qq\tau\nu(\gamma)$	20	3.1	$3.10 \pm 1.05 \pm 0.13$	2.50 ± 0.01
$\mathrm{e^+e^-} \to qqqq(\gamma)$	75	13.9	$8.35 \pm 1.22 \pm 0.15$	7.82 ± 0.04

Table 3: Number of selected data events, N_{data}, number of expected non-W background events, N_{bg}, and CC03 cross sections for the reactions $\mathrm{e^+e^-} \to qq\mathrm{e}\nu(\gamma)$, $\mathrm{e^+e^-} \to qq\mu\nu(\gamma)$, $\mathrm{e^+e^-} \to qq\tau\nu(\gamma)$, $\mathrm{e^+e^-} \to \ell\nu\ell\nu(\gamma)$ and $\mathrm{e^+e^-} \to qqqq(\gamma)$ at the three different centre-of-mass energies. For the $qqqq$ signal, the numbers N_{data} and N_{bg} correspond to a cut on the output of the neural network at 0.8, while the $qqqq$ cross section is obtained from a fit to the neural-network output distribution as described in Section 2.5. The first error is statistical and the second systematic. Also shown are the SM CC03 cross sections, σ_{YFSWW3}, as calculated with YFSWW3 [29]. The theoretical error on the YFSWW3 cross sections amounts to 0.5% [29].

Parameter	Lepton Non-Universality	Lepton Universality	Standard Model
$B(\mathrm{W} \to \mathrm{e}\nu)$ [%]	$10.40 \pm 0.26 \pm 0.14$	—	
$B(\mathrm{W} \to \mu\nu)$ [%]	$9.72 \pm 0.27 \pm 0.15$	—	
$B(\mathrm{W} \to \tau\nu)$ [%]	$11.78 \pm 0.38 \pm 0.21$	—	
$B(\mathrm{W} \to \ell\nu)$ [%]	—	$10.55 \pm 0.13 \pm 0.11$	10.83
$B(\mathrm{W} \to qq)$ [%]	$68.10 \pm 0.41 \pm 0.33$	$68.34 \pm 0.40 \pm 0.33$	67.51

Table 4: W-decay branching fractions, B, derived with and without the assumption of charged-current lepton universality. The correlations between the leptonic branching fractions are -0.016, -0.279, -0.295 for (eμ), (eτ), ($\mu\tau$), respectively. Also shown are the W-decay branching fractions [3] as expected in the Standard Model.

$\sqrt{s}$ [GeV]	$\sigma_{\ell\nu\ell\nu}$ [pb]	$\sigma_{qq\ell\nu}$ [pb]	σ_{qqqq} [pb]	σ_{WW} [pb]
204.82	$1.55 \pm 0.22 \pm 0.07$	$7.63 \pm 0.38 \pm 0.13$	$8.06 \pm 0.39 \pm 0.15$	$17.35 \pm 0.58 \pm 0.24$
206.48	$1.51 \pm 0.16 \pm 0.07$	$7.77 \pm 0.30 \pm 0.13$	$8.51 \pm 0.31 \pm 0.15$	$17.91 \pm 0.46 \pm 0.24$
208.00	$2.44 \pm 0.80 \pm 0.11$	$8.06 \pm 1.16 \pm 0.14$	$8.35 \pm 1.22 \pm 0.15$	$18.69 \pm 1.83 \pm 0.24$

Table 5: CC03 cross sections for the reactions $\mathrm{e^+e^-} \to \ell\nu\ell\nu(\gamma)$, $\mathrm{e^+e^-} \to qq\ell\nu(\gamma)$ (summed over lepton species), $\mathrm{e^+e^-} \to qqqq(\gamma)$, and the total W-pair cross section, σ_{WW}, as resulting from the fits to the data at the three centre-of-mass energies. The total W-pair cross sections as expected in the Standard Model, calculated with YFSWW3 [29], are 17.13 pb, 17.14 pb, and 17.15 pb respectively at the three centre-of-mass energies. These values are consistent with the predictions from the RacoonWW [30] program and their theoretical errors amount to 0.5%.

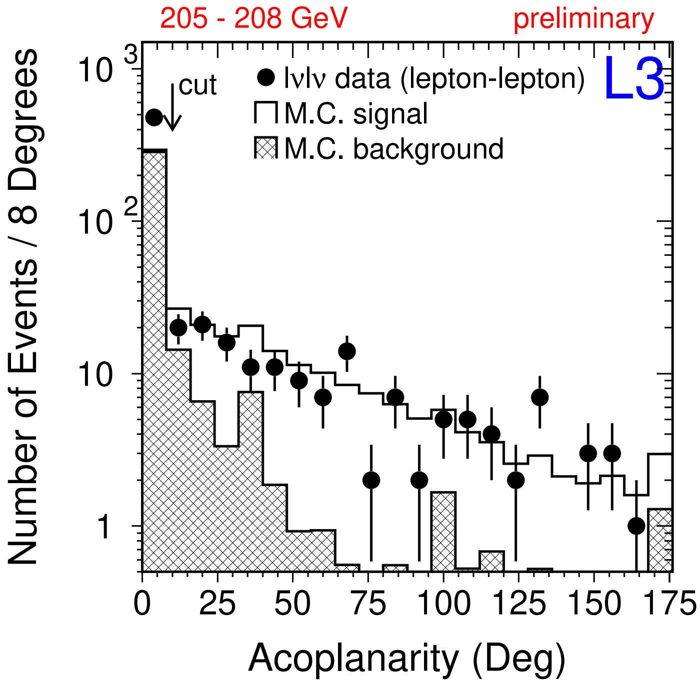

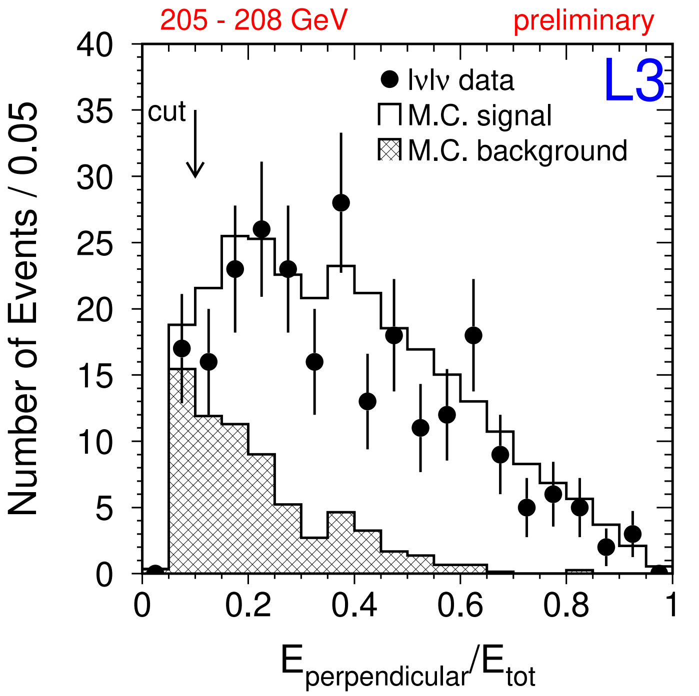

Figure 1: Distributions of variables used for the selection of $e^+e^- \to \ell\nu\ell\nu(\gamma)$ events, comparing the signal and background Monte Carlo to the data. The position of the selection cuts are indicated by vertical arrows. All selection cuts except in the variable plotted are applied. (a) The acoplanarity between the two leptons in the lepton-lepton class. (b) The energy imbalance in the plane transverse to the beam direction normalised to the visible energy.

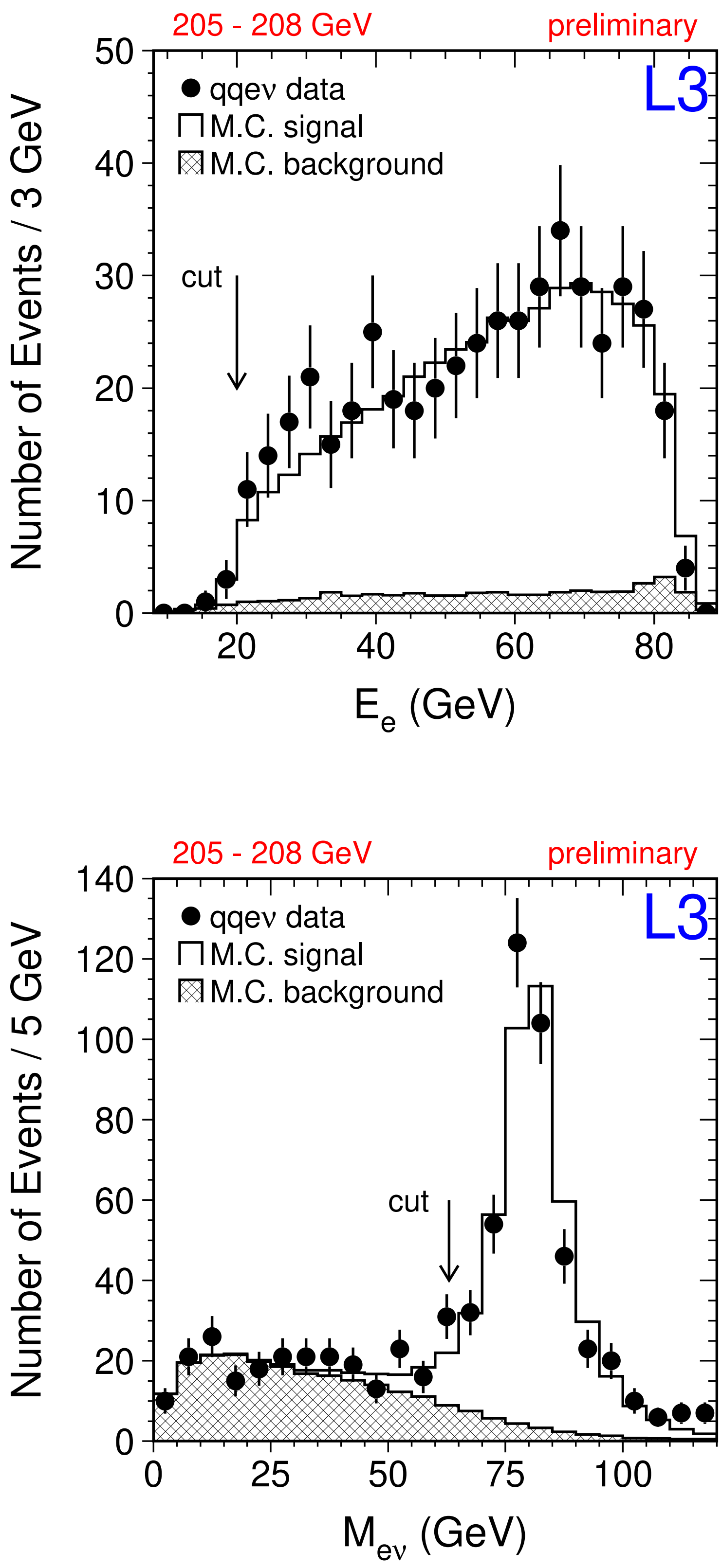

Figure 2: Distributions of variables used for the selection of $e^+e^- \rightarrow qqe\nu(\gamma)$ events. (a) The energy of the electron E_e. (b) The invariant mass of the electron-neutrino system, $M_{e\nu}$.

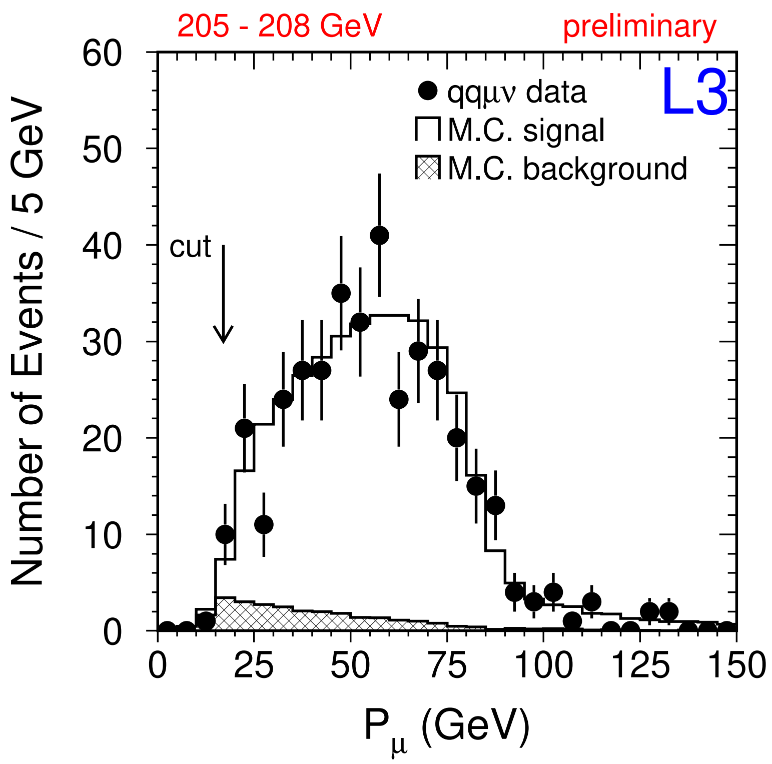

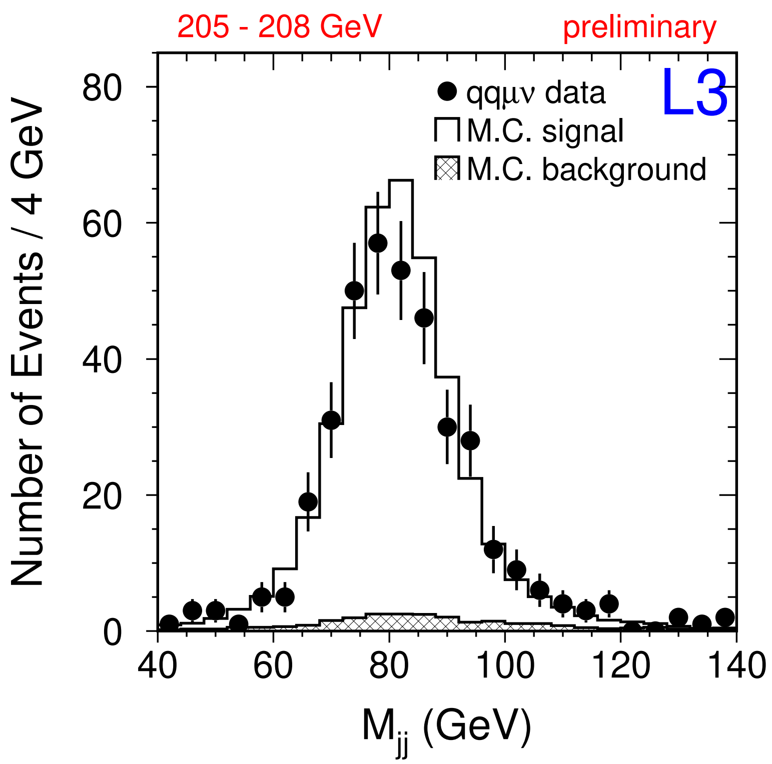

Figure 3: Distributions of variables used for the selection of $e^+e^- \to qq\mu\nu(\gamma)$ events. (a) The momentum of the muon p_μ. (b) The invariant mass of the jet-jet system, M_{jj}.

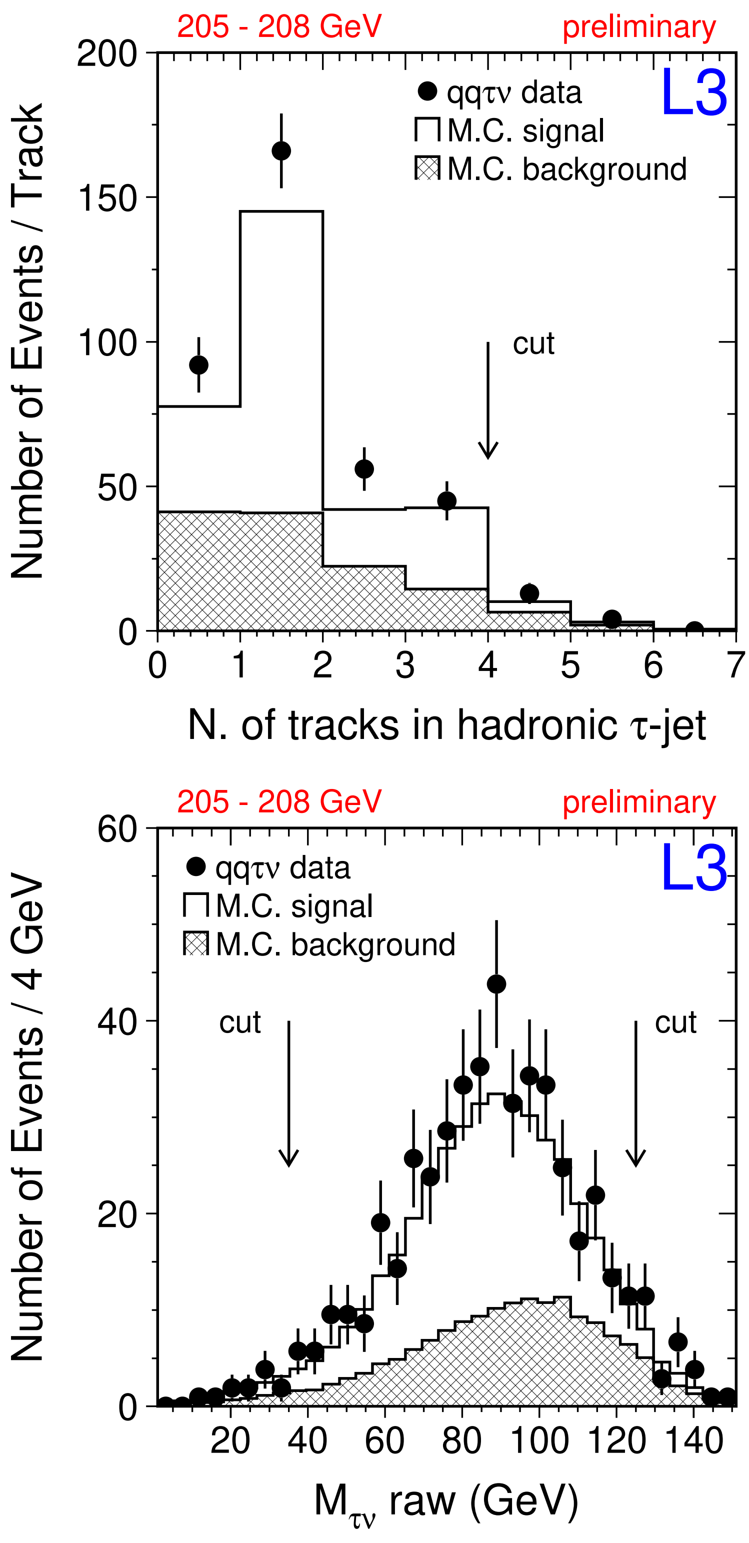

Figure 4: Distributions of variables used for the selection of $e^+e^- \to q q \tau \nu(\gamma)$ events. (a) The number of TEC tracks associated to the τ jet. (b) The invariant mass of the tau-neutrino system, $M_{\tau\nu}$.

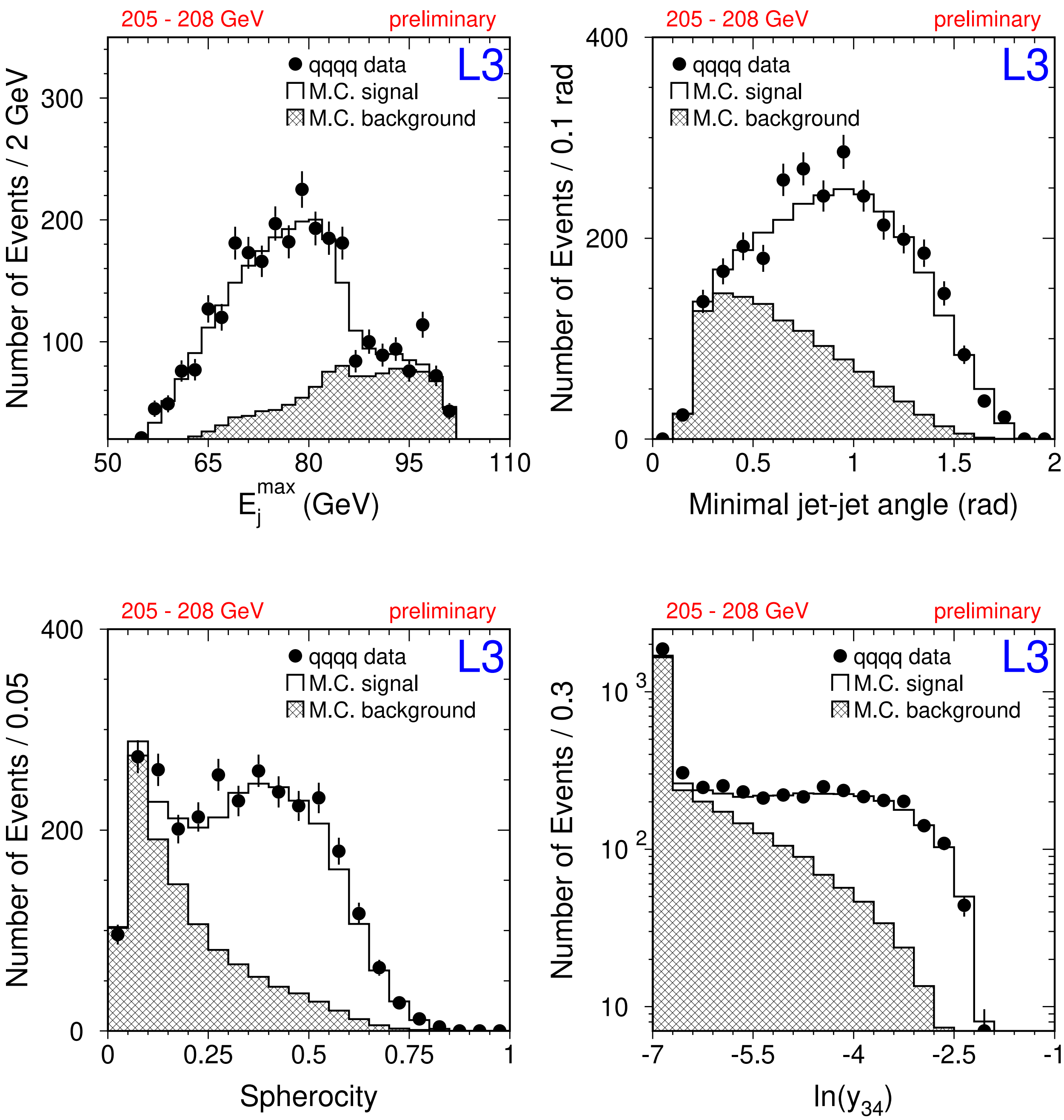

Figure 5: Distributions of variables used for the neural network in the analysis of $e^+e^- \rightarrow qqqq(\gamma)$ events or describing the event shape of the hadronic final state. All selection cuts are applied. (a) The maximal jet energy. (b) The minimal jet-jet opening angle. (c) The spherocity. (d) $\ln y_{34}$.

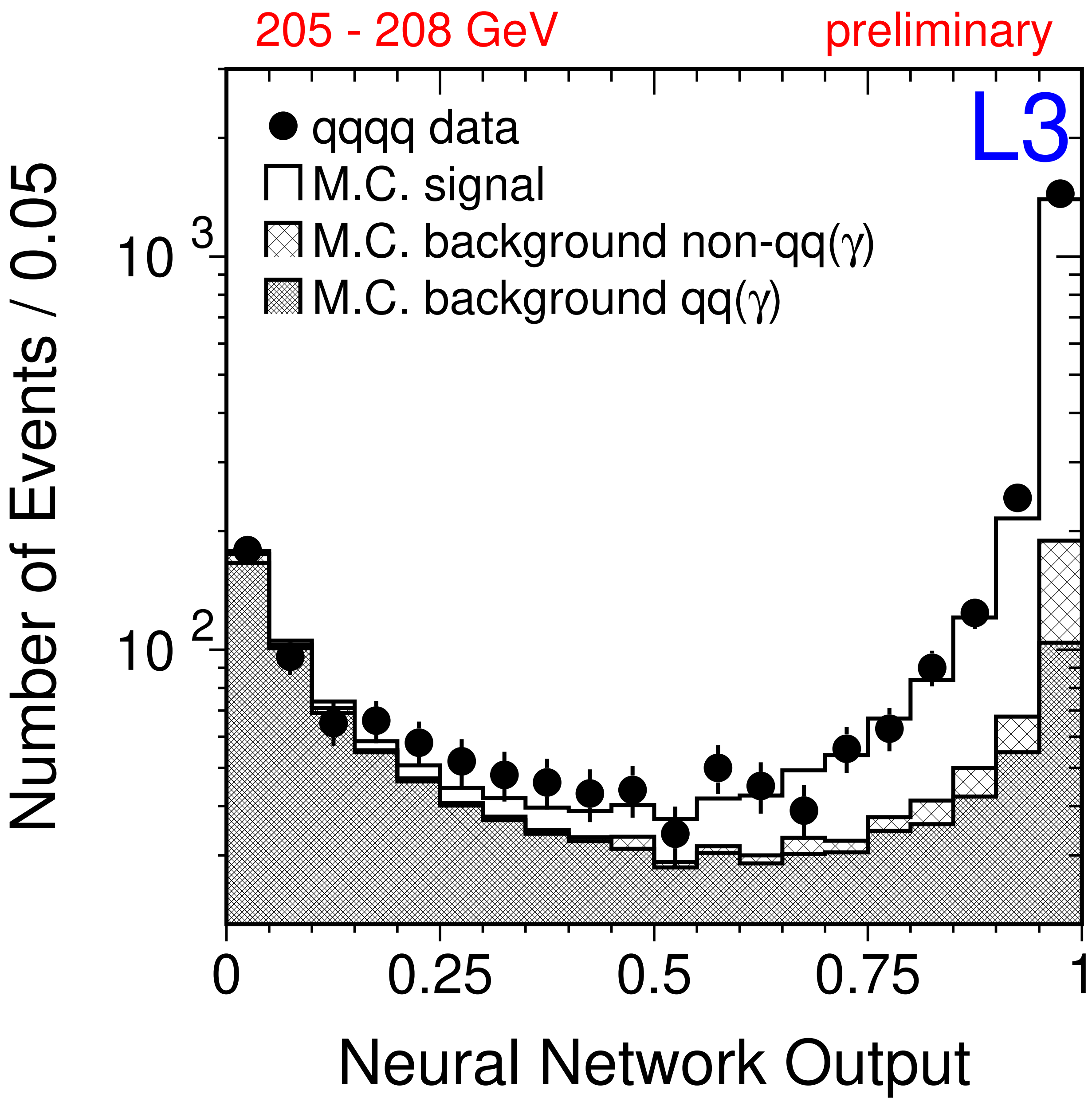

Figure 6: Distribution of the output of the neural network used in the analysis of $e^+e^- \rightarrow qqqq(\gamma)$ events.

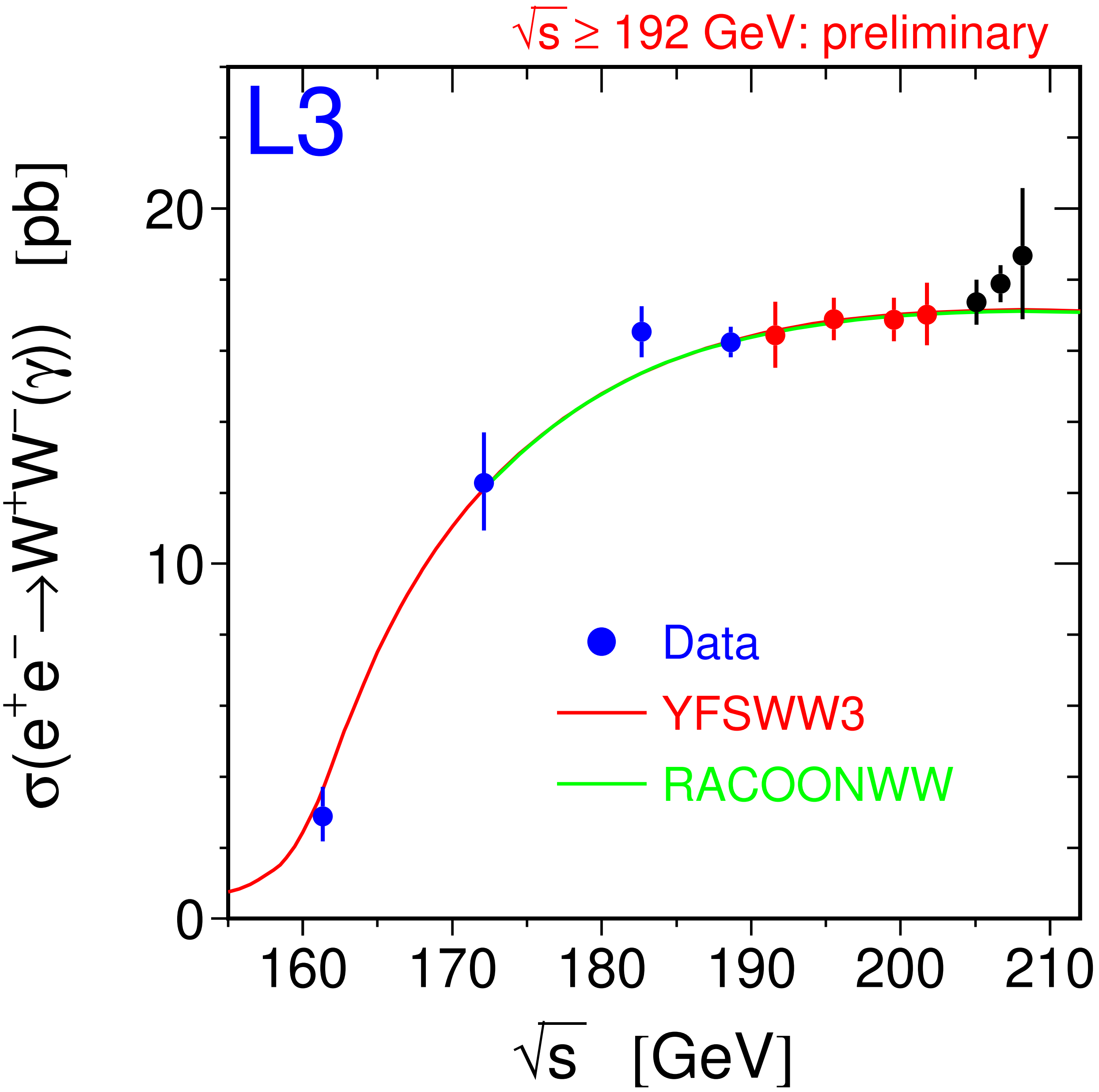

Figure 7: The cross section, $\sigma_{\rm WW}$, of the process $\rm e^+e^- \rightarrow WW \rightarrow \mathit{ffff}(\gamma)$ as a function of the centre-of-mass energy, $\sqrt{s}$. The published measurements of $\sigma_{\rm WW}$ at $\sqrt{s}$ of 161 GeV, 172 GeV, 183 GeV, 189 GeV, the preliminary measurements at $\sqrt{s} = 192 - 202$ GeV, and the new preliminary measurements at $\sqrt{s} = 205 - 208$ GeV are shown as dots with error bars, combining statistical and systematic errors in quadrature. The overlapping solid curves show the Standard Model expectation as calculated with YFSWW3 [29] in the whole energy range and RacoonWW [30] for $\sqrt{s} \geq 170$ GeV. The theoretical error on these predictions amounts to 2.0% in the threshold region going down to 0.5% [3,4] for $\sqrt{s} \geq 170$ GeV.

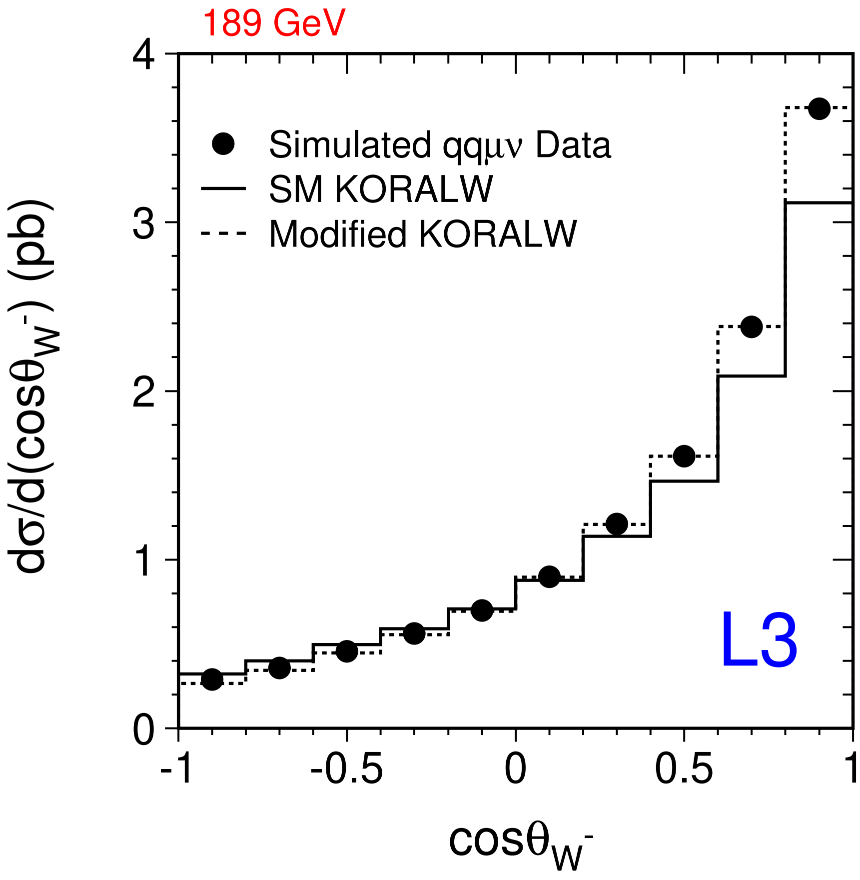

Figure 8: A simulated event sample (dots), obtained re-weighting a SM Monte Carlo distribution by a linear distortion in $\cos\theta_{\mathrm{W}^-}$, is treated as real data. The modified Monte Carlo distribution (dashed line) and the original distribution (solid line) used for the bin-by-bin correction are also shown.

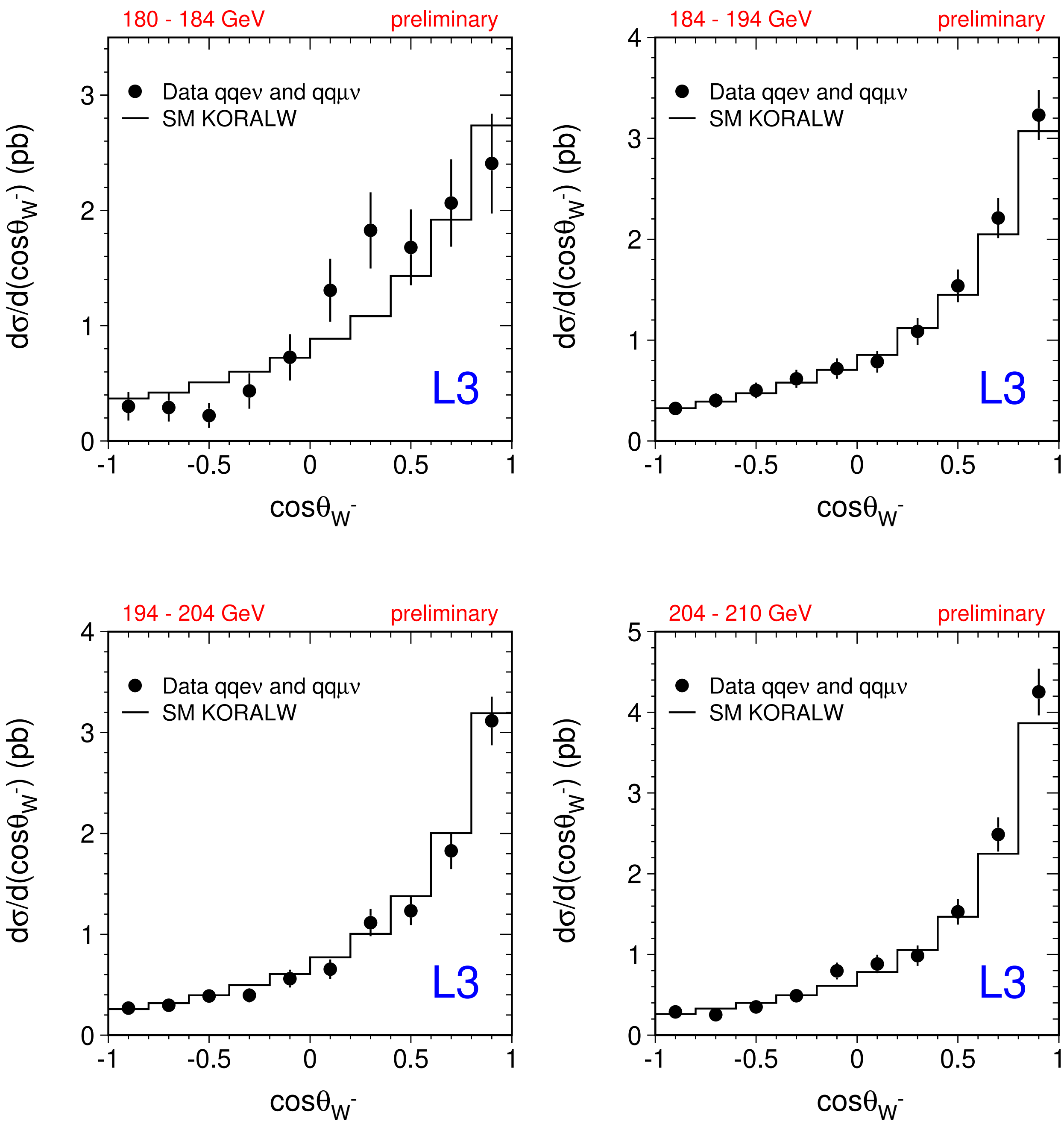

Figure 9: Measured differential cross sections as a function of $\cos\theta_{W^-}$ using the full $qqe\nu(\gamma)$ and $qq\mu\nu(\gamma)$ statistics. The cross sections are averaged assuming lepton universality. Experimental data (dots) are compared to Monte Carlo expectations (solid lines).